Effect of substrate bias voltage on defect generation and their influence on corrosion and tribological properties of HIPIMS deposited CrN/NbN coatings

BISWAS, Barnali, PURANDARE, Yashodhan <http://orcid.org/0000-0002-7544-9027>, KHAN, Imran and HOVSEPIAN, Papken <http://orcid.org/0000-0002-1047-0407>

Published version

BISWAS, Barnali, PURANDARE, Yashodhan, KHAN, Imran and HOVSEPIAN, Papken (2018). Effect of substrate bias voltage on defect generation and their influence on corrosion and tribological properties of HIPIMS deposited CrN/NbN coatings. Surface and Coatings Technology, 344, 383-393.

Effect of substrate bias voltage on defect generation and their influence on corrosion and tribological properties of HIPIMS deposited CrN/NbN coatings

Barnali Biswas [a,1], Yashodhan Purandare [1], Imran Khan [2] and Papken Eh. Hovsepian [1]

[1]National HIPIMS Technology Centre, Materials and Engineering Research Institute, Sheffield Hallam University, City Campus, Howard Street, Sheffield S1 1WB, United Kingdom

[2]Zimmer-Biomet UK Limited, Dorcan Industrial Estate, Murdoch Road, Swindon SN3 5HY, United Kingdom

[a)] Corresponding author: Barnali.Biswas@student.shu.ac.uk , bbbbarnali@gmail.com

Abstract: Substrate bias voltage is one of the most influential deposition parameter for physical vapour deposition processes as it can directly control the adatom mobility during coating growth. It influences the hardness, roughness as well as the microstructure of the coatings. Thus, bias voltage could also affect the defect formation during the coating deposition. High Power Impulse Magnetron Sputtering (HIPIMS) has been proven useful in producing void free and arc droplet free dense coatings. However, such coatings can still suffer from some defects associated with external factors (independent of deposition technique), such as substrate irregularities and the flakes coming from the chamber components. In order to study the effects of bias voltage (U_b) on the defect formation during HIPIMS process, four sets of CrN/NbN coatings were deposited at U_b = - 40 V, - 65 V, - 100 V and - 150 V. Microscopic studies revealed that with the increase in bias voltage the coatings morphology was altered and the percentage of surface area covered by optically visible defects was increased from 3.13 % to 4.30 %. The defects on the coatings deposited at U_b = - 100 V and - 150 V led to preferential corrosive attack resulting in a sharp increase in corrosion current density during Potentiodynamic polarisation experiments. Room temperature pin-on-disc tribological tests exhibited the influence of defects on the wear behaviour; however, the coefficient of friction (μ) values were mainly influenced by the

nature of the oxides formed during the tests. Coating microstructure and bilayer thickness, along with the coating defects determined the coefficient of wear (Kc) values. This study revealed that the coating deposited at U_b = - 65 V had the highest wear resistance (Kc = 2.68 $\times 10^{-15}$ $m^3N^{-1}m^{-1}$) and the lowest friction (μ = 0.48).

1. Introduction

In recent years, the attention towards CrN/NbN multilayer coatings produced by physical vapour deposition (PVD) is growing rapidly due to their advanced barrier properties against corrosion and wear [1–6]. Moreover, use of the novel High Power Impulse Magnetron Sputtering (HIPIMS) deposition technique to deposit CrN/NbN coatings is found to be beneficial in improving those properties [7–9]. The enhancement in the coating properties can be attributed to superior microstructure due to the high ion to neutral ratio and the low average power during the HIPIMS process [10–12]. The trajectories of ions can be controlled by applying external electric and magnetic fields. Thus, using HIPIMS technique it is possible to produce homogeneous coatings, even on complex-shaped substrates [13,14]. However, higher ion content also has a disadvantage. The back attraction of the positively charged metal ions to the target reduces the deposition rate during the HIPIMS process. Combining HIPIMS with the Unbalanced Magnetron Sputtering (UBM) process can eradicate this problem and improve the deposition rate [15].

Previous research showed that the coatings produced by HIPIMS technique are free from droplet related defects when operated under carefully selected parameters, such as the right frequency, pulse width and arc suppression settings [9–12,15]. However, HIPIMS deposited coatings can still suffer from surface imperfections, i.e. coating defects which are associated with external factors, such as substrate pits and the flakes generated from the chamber components [9,16] and are independent of deposition technique. Unlike arc droplets, these defects grow along with the coatings [9]. It is well known that the coating growth is influenced by the deposition parameters such as deposition time, substrate temperature and chamber pressure [9,14,16–19]. Thus, the defect growth gets influenced by these parameters indirectly [9,16]. The substrate bias voltage is another important deposition parameter because it controls the adatom mobility during coating growth [20–26]. Therefore, the study

of the influence of bias voltage on the formation of morphological defects is the particular research interest.

Coating defects are undesirable because they degrade the coating properties [1,6,9,16,27–30]. For example, metallic droplets can augment wear by acting as protruding asperities when intact with the coating or they can initiate three body abrasion if loose [31]. Coating imperfections like pores, holes and voids either present inherently or generated by the removal of droplet and nodular defects, can expose the substrate to the corrosive media and accelerate the corrosion process [1,6]. As the coating industries are continually growing and developing, there is a demand for improved and long lasting coatings for advanced applications such as coating on biomedical devices. Therefore, it is much needed to understand the formation of coating defects and their influence on coating performance in order to improve coating properties and durability.

The influence of HIPIMS on coating microstructure and mechanical properties has been studied recently [7–15,32,33]. Literature lists very few studies which describe defect generation in coating deposited by HIPIMS. Previous studies by the authors reported the effect of deposition time and the total chamber pressure on the external factors which lead to the generation of defects [9,16]. This study further investigates the effect of bias voltage on these influences in detail.

2. Experimental details

2.1. Coating deposition

Nanostructured CrN/NbN multilayer coatings were deposited in an industrial sized (1 m^3) Hauzer 1000 four cathode PVD machine which was facilitated with HIPIMS power supplies (Hüttinger Elektronik Sp. z o.o., Warsaw, Poland) and an advanced bias power supply with active arc suppression units. 304 stainless steel coupons, M2 high speed steel coupons and (100) Silicon wafer were used as substrates. All the substrates were mounted on a rotating substrate holder, located at the centre of the deposition chamber with a three-fold rotational motion of the substrate holder. Prior to coating deposition, the sample surfaces were pre-treated by HIPIMS plasma discharge enriched with Cr ions to increase the adhesion of the coating with the substrate [34]. Then the coatings were deposited for 120 min using combined HIPIMS and UBM techniques [15] at a temperature of 200 °C. Four sets of coatings were produced by varying the bias voltage, namely - 40 V, - 65 V, - 100 V and - 150 V. During the deposition processes, one Cr and one Nb target were operated in HIPIMS mode and the other two targets (1 Cr and 1 Nb) were operated in UBM mode. The applied power on an individual cathode was maintained at 8 kW irrespective of the technology (UBM or HIPIMS). Rectangular pulses of 200 µs at a frequency of 100 Hz, with a duty cycle of 1 % were employed to generate the HIPIMS plasma for coating deposition. Ar and N_2 (1:1) were used as the process gas and the chamber pressure was maintained at 0.35 Pa.

Note that the coating produced at U_b = - 65 V was used in our earlier reports also [9,16].

2.2. Coating characterisation

In order to investigate the effect of bias voltage on defect generation, Scanning Electron Microscopy (FEI NOVA-NANOSEM 200) was employed as the primary characterization

technique in this study. Using ETD (Everhart-Thornley detector) and TLD (Through the Lens Detector), the SEM images of planar and fractural cross-sectional view of the coatings were captured at low and high magnifications respectively. The surface area of the coating covered by the defects was determined from optical microscopic images (captured by Huvitz 3D Metallurgical Microscope). Then the relative area covered by defects (in percentage) was analysed from binary pictures using ImageJ software [9]. Surface roughness of the coatings was measured by a DEKTAK 150 stylus profilometer. For each scan, the probe travelled a length of 1000 μm and the surface roughness of the scanned profile was calculated by the associated software.

Corrosion behaviour of the CrN/NbN coatings was examined using a Gill AC Potentiostat. Coated 304 stainless steel samples were polarized from −1000 to +1000 mV at a scan rate of 0.5 $mVsec^{-1}$ in a 3.5 % NaCl solution. The samples were masked using bee's wax to expose only an area of 1 cm^2 to the solution.

A CSM room temperature pin-on-disc tribometer in dry sliding conditions was used to study the friction behaviour of the coatings deposited by varying the bias voltage. CrN/NbN coated M2 high speed steel samples were used for these experiments. Each test was run for 20000 cycles. In order to measure friction rates, a 5 N static load was applied on the counterpart (Al_2O_3 ball of 6 mm diameter). A Horiba-Jobin-Yvon LabRam HR800 integrated Raman spectrometer fitted with a green laser (wavelength, 532 nm) was used to study the chemistry of the tribolayer formed at the tribological contacts. In addition, X-ray Diffraction technique in high angle (2θ, 20° - 100°) and low-angle (2θ, 2° - 10°) geometry (LAXRD) was used to evaluate the crystallographic structure and the bilayer thickness of these coatings respectively. The coating hardness was determined from the loading-unloading curves obtained from a CSM nanoindentation tester. More details about coating deposition and characterisation techniques can be found elsewhere [9,16].

3. Results and discussion

3.1. Coating morphology and microstructure

Fig. 1 (a-h) shows the planar and cross-sectional SEM images of the coatings, which were used to study the coating morphology and microstructure.

The coating deposited at - 40 V substrate bias exhibited a columnar structure with rounded columnar tops (Fig. 1a,b). With an increase of bias voltage from - 40 V to - 65 V, coalescence of adatoms increased leading to an increase in density of columnar grains (Fig. 1c); however, retaining the columnar morphology (Fig. 1d) as in the case of lower bias voltage. As the bias voltage was further increased to - 100 V, columnar grains appeared widened (Fig. 1e) due to the high adatom mobility leading to grain coarsening. Fig. 1f shows the cross-sectional view of this coating (U_b = - 100 V) which clearly exhibits the influence of increasing bias voltage on microstructure densification. The column microstructure in the case of the coating deposited at U_b = - 150 V was even harder to resolve giving an impression of a bulk material (Fig. 1g,h). The changes in the coating microstructure and surface morphology with the bias voltage can be attributed to the increased surface mobility of adatoms on the growing film [20–26].

Table 1 shows the thickness of the coating measured from the cross-sectional SEM images. As expected, deposition rate increased when bias voltage was increased from - 40 V to - 65 V. However, further increase in the bias voltage led to re-sputtering of the depositing materials thereby resulting into a slight decrease in the coating thickness. For the coating deposited at U_b = - 150 V, strong re-sputtering process resulted in the lowest thickness of 1.80 µm even though all other deposition parameters were kept constant. Fig. 1g shows this re-sputtering effect observed for - 150 V coating. The dome shaped feature usually observed for sputtered coating is completely absent here, rather the coatings surface exhibits dents

resulted from the sputtering of materials from the coating surface. Moreover, densification of microstructure could also lead to a slight decrease in the coating thickness. As observed in the Fig. 1g,h this coating became densified due to the increase of adatom mobility with the increase of negative substrate bias voltage.

3.2. Growth defects

The SEM study on coating morphology and microstructure exhibited a number of morphological defects of various shapes and sizes. Depending on their origins, these defects were categorised into two groups; flakes related defects and defects associated with substrate pits (namely, pinhole defects). The types of defects identified in HIPIMS/UBM coatings were very similar in nature to those reported earlier for a conventional magnetron sputtering process [27].

Flakes related defects are found in most coatings deposited in a vacuum chamber. These flakes can be generated due to the thermal and structural stresses on the chamber components (shields, heaters) during coating deposition [27]. The bombardment of the chamber components by highly ionised flux and the rotation of the substrates holders during deposition can also produce some seed particles within the chamber[9]. Due to the deposition of coating materials on the flakes attached to the substrate, nodular shaped defects (Fig. 2a,b) are formed.

During or after the deposition, thermal or mechanical stresses can deform and delaminate these defects from the coating and create voids. These voids are called open void defects (Fig. 2c). Fig. 2d shows a pinhole defect in the coating which is associated with the substrate surface imperfections, such as small craters, pits etc. Deposition of coating materials can cover most of the surface imperfections. However, larger cavities may not be closed fully and remain as pinholes within the coatings.

In detail observation of the SEM images of a nodular shaped defect on HIPIMS/UBM coating (Fig. 2a,b) reveal that the columnar morphology of these defects and the surrounding coatings is similar; except for the interruption in the continuity caused by the contamination at the surface before/during deposition. This indicates that the growth mechanisms for the surrounding coatings and these defects are similar and they grow over the course of time just like the coating. Moreover, EDX analysis confirms (Fig. 3a,b) that the elemental compositions of the nodular defect are also same as coating. Atomic percentages of Cr, Nb and N were found to be 39 %, 14 % and 47 % respectively for both the coating and the nodular defect. This emphasises that defects in HIPIMS/UBM coatings are generated due to the deposition of coating materials on flakes and not due to arcs.

For comparison, SEM image of a droplet on commercially available arc-PVD CrN/NbN coating has been included. Significant differences in morphologies and sizes between the arc droplet and the nodular defect can be seen from the Fig. 2a and 3a,c. The arc droplet is bigger in size and has a continuous solid structure whereas in comparison the grain boundaries and columnar coating growth on a nodular defect in the case of HIPIMS/UBM coating could be clearly observed from the higher magnification image of the nodular defect (Fig. 2a).

Moreover, Fig. 3c also exhibits the morphological differences between the arc deposited coating surface and arc droplet which suggests that the growth steps of the coating and the droplet are different. Most likely, an instant solidification of cluster of materials ejected from the target leads to droplet formation in arc-PVD. EDX analysis (Fig. 3d) shows that the droplet is mostly made of Cr indicating that this droplet is generated due to the expulsion of molten Cr from Cr target at the cathode spot.

3.3. Surface defect density calculation

SEM images revealed that all the coatings had similar type of defects on them, but the number of defects increased with the increase of bias voltage. To quantify the defect population, statistical measurement of number of defects were carried out using optical microscopy and Image J software [9]. In this study, the percentage of surface area covered by optically visible defects was termed as surface defect density (A_d). Fig. 4a shows an image of the coating surface captured by an optical microscope and Fig. 4b represents the variation of surface defect density as a function of substrate bias voltage (& converted binary images of the coatings in the insets).

The calculated defect densities (A_d) of the coatings deposited at bias voltages of - 40 V and - 65 V were similar (3.13 % and 3.18 % respectively). Whereas, a sudden increase in A_d value (4.14 %) was observed when a higher bias voltage (U_b = - 100 V) was applied to the substrate.

The increase of the surface area coved by optically visible defects with the increase in substrate bias is believed to be associated with two factors. At higher bias voltages, the high-energy flux bombardments on chamber components can increase the flakes generation. These flakes can produce more defects in the coating. Nevertheless, re-sputtering phenomena can also be responsible for raising the surface defect density. At high negative bias voltages, the high-energy bombardment on the growing coatings can expose the already formed defects and hence increase the area under the defects. Also, some loosely bound nodular defects can be expelled from the coatings leaving more visible voids.

In the optical images, the surface imperfections, i.e., both the protrusions and pits are seen as dark features. Therefore, it was not possible to quantify the number of flakes related defects and the number of pinhole defects. However, extensive SEM studies of substrate and coating defects indicated that all the dark features observed on the substrate were substrate pits (Fig.

4c) whereas along with some pinhole defects/voids, higher number of nodular shaped defects were observed on the surface of the coatings. The defect density calculation also revealed that A_d value of the substrate was only 0.39 ± 0.04 which was purely due to the presence of substrate pits. Thus, it could be concluded that most of the defects observed on the surface of the coatings were originated due to the deposition of coating materials on the flakes.

Apparently, in this study the HIPIMS/UBM coating with highest number of defects had lesser defects as compared to that of commercially available arc-PVD CrN/NbN coating. Fig. 4d shows the surface of this arc-PVD CrN/NbN coating. The analytical calculation releveled that 11 ± 0.48 % of its surface is covered by the defects, most of which are the droplet defects.

3.4. Roughness

The roughness values of the coatings are summarised in Table 2. As seen from the table, roughness values of the coatings deposited at bias voltages of - 40 V and - 65 V were similar. When the bias voltage increased from - 65 V to - 100 V, the roughness of the coating increased abruptly reaching the highest value (0.083 µm). Further increase in bias voltage to - 150 V, decreased the roughness to 0.073 µm.

This result shows consistency with the surface defect density values of the coatings. The increase in surface defect density with the increase of bias voltage resulted in rougher surfaces. Thus, the roughness value suddenly increased from 0.039 to 0.83 µm when the bias voltage was raised from - 65 V to - 100 V. However, there was a slight decrease in roughness value from 0.083 to 0.073 µm when bias voltage was increased from - 100 V to - 150 V. This could be attributed to the densification of the coating, as the dome shaped columnar tops disappeared (Fig. 1g). Thus, it can be concluded that the roughness of the coating was associated to the surface defect density as well as to the features of the coating morphology.

3.5. Potentiodynamic polarisation experiment

Fig. 5. shows the Potentiodynamic polarisation curves of the coatings deposited by varying bias voltage. It was clear from the curves that the increased substrate bias improved the corrosion resistance of the coatings. As observed from the SEM images (Fig. 1), increased negative bias densified the coating. Thus, the higher corrosion resistance of the coatings was attributed to the densification of coatings with the increase of substrate bias voltage.

In the anodic potential ranging from - 250 mV to + 475 mV, the corrosion current density was notably higher (one order of magnitude) for the coating deposited at - 40 V bias voltage than the coatings deposited at higher bias voltages (- 100 V and - 150 V). Although surface defect density of this coating (U_b = - 40 V) was the lowest (A_d = 3.13%), the under-dense structure of the coating may deteriorate the corrosion resistance. The coatings deposited at higher substrate bias voltages ($\geq$ - 65 V) exhibited similar corrosion current values in the potential range of 0 mV to + 350 mV which suggested that - 65 V can be used as the optimum bias voltage to produce dense coatings for corrosion applications.

Apparently, the effect of the higher number of defects on coating corrosion performance was also observed. The coating deposited at bias voltage of - 100 V and - 150 V had higher defect densities (4.14 % and 4.30 %) and the polarisation curves of both coatings evidenced the formation of metastable pits which are believed to be associated with the growth defects. The gaps between loosely bound defects and the coating act as solution-paths which initiate the galvanic and crevice corrosion between the coating and the substrate [6,35]. The dissolution of metals at the defect sites due to the galvanic effects could lead to the removal of defects and expose the fresh substrate surface to the corrosive media. As a result, electrochemical reaction kinetics was raised which was observed by the sharp increase in current densities in the anodic potential range, at around 300 mV and 50 mV for the coatings deposited at U_b = - 100 V and - 150 V respectively.

3.6 Tribological properties

A Room Temperature Pin-on-disc tribometer was used to study the friction behaviour of the deposited coatings in dry sliding condition. Fig. 6 shows the dependence of friction coefficient on number of revolutions (friction cycles) for the coatings deposited by varying bias voltage.

The influence of surface defect density on coefficient of friction, COF (μ) values was not apparent. The coating deposited at - 65 V had the lowest μ value of 0.48. There was a sudden drop in the value of μ around a friction cycle of 4000. This test was conducted three times. Each time, the coating exhibited similar behaviour. The surface defect density values of the coatings deposited at - 40 V, - 100 V and - 150 V were different, however, they all showed similar friction behaviour and had similar μ values.

As suggested by the previous research [4,5,16], the friction values can depend on the oxides produced during the tribological tests. Thus, to better understand the friction behaviour of the coatings, Raman spectra from the wear tracks were obtained using a Raman spectrometer (Fig. 7).

The Raman spectra from the wear tracks of the coatings deposited at U_b = - 100 V, - 150 V exhibited a pronounced peak at 790cm^{-1} which is a characteristic of $CrNbO_4$ [5,36] and both the coatings had similar friction values (μ = 0.65 and 0.68 respectively). The coatings produced at U_b = - 40 V and - 65 V showed similar types of Raman spectra expect the intensity of the peaks were higher, especially the peak at around 835 cm^{-1} was much higher for the coating deposited at U_b = - 40 V. This could be due to the production of Nb_2O_5 , nH_2O [5,36] which could also lead to an increase in μ value of the coating deposited at U_b = - 40 V. This study suggested that the friction values of these coatings were mainly controlled by the produced oxides.

The difference in oxidation behaviour during the tribological tests could be associated with their stoichiometry and/or crystallographic orientation [37–40]. The change in the stoichiometry due to the preferential re-sputtering of coated flux at different bias voltages caused the variation between the chromium nitride and niobium nitride layers in the structure [41]. As a result, the crystallographic orientation of the coatings was changed (Fig. 8). The coating deposited at - 65 V, displayed a pronounced (111) orientation of nitride phase and this coating showed higher oxidation resistance during sliding (supported by Raman spectra). Whereas all other coatings (deposited at - 40 V, - 100 V, - 150 V) with (200) preferred orientation were easily oxidised. The reason for this differences in oxide growth rate was suggested to be associated with surface energy of the different grain structures [37].

In case of Titanium nitride coating (TiN) also (111) oriented grains showed higher oxidation resistance [42]. Whereas production of oxides was evident on (220) TiN orientated coatings. However, (220) orientated TiN coatings had lower μ values than the (111) orientated TiN coatings. This is because the oxide produced on (220) orientated coatings was Ti_nO_{2n-1} which belongs to Magnéli family [43], i.e., it has easily shearable atomic planes and therefore it is lubricious.

In contrast, Nb-rich tribolayers were formed on (200) orientated coatings. $CrNbO_4$ and Nb_2O_5 , nH_2O are not luricious and especially Nb_2O_5 , nH_2O is known as non-protective oxide [5]. For this reason higher μ values were observed for the coatings deposited at U_b = - 40 V, - 100 V, - 150 V. The coating produced at U_b = - 65 V also showed several peaks which might correspond to Cr_2O_3, $CrNbO_4$ and Nb_2O_5 , nH_2O [5,36] but none of them was intense. Thus it could be concluded that the higher oxidation resistance during sliding led to lowest μ value of 0.48 in case of the coating deposited at U_b = - 65 V.

However, CrN/NbN coating has multilayer structure which makes the oxidation behaviour during sliding progress more complex than any single layer coating, for example TiN coating.

Thus, more systematic study about the oxidation properties of each grain orientation and individual layer is required to understand the friction behaviour of CrN/NbN coatings in detail, and can be a topic of future research.

The coefficient of wear, COW (K_C) of the coating was calculated using the profilometer data of the wear track (Fig. 9). K_C was found to be the highest (4.19×10^{-15} $m^3N^{-1}m^{-1}$) for the coating deposited at the lowest bias voltage of - 40 V. Due to the under-dense columnar structure, large amount of material was removed from this coating during sliding. Fig. 10a shows the debris in the wear track (dark contrast) generated due to the removal of coating materials. With the increase of bias voltage from - 40 V to - 65 V, a significant improvement in wear resistance was observed ($K_C = 2.68 \times 10^{-15}$ $m^3N^{-1}m^{-1}$ for - 65 V). This could be attributed to the strong interactions between the columns which provided effective protection against spalling and thus reducing the material removal rate of the coating [44].

Further increase of the bias voltage was found to be ineffective in enhancing the wear resistance; rather, it degraded the wear properties. As discussed earlier, the application of higher bias voltage ($\geq$ - 100 V) increased the surface defect density. Due to the height of the nodular defects (nodular/cone-like), they are subjected to a full contact during sliding [28]. As a result, the nodular/cone-like defects experience high stresses which cause their fracture and spalling. The debris generated from the nodular defects creates tribological film within the wear tracks. Moreover, poorly attached nodular defects could be totally pulled out and increase the wear debris formation. Due to the generation of debris from the defects, wear rates of the coatings deposited at - 100 V and - 150 V substrate bias increased ($K_C = 3.36 \times 10^{-15}$ $m^3N^{-1}m^{-1}$ and 3.85×10^{-15} $m^3N^{-1}m^{-1}$ respectively).

Fig. 10c,d represents the wear tracks of these coatings (- 100 V and - 150 V) which clearly shows that the number of voids (black dots) generated due to the removal of defects are higher compared to other two coatings (- 40 V and - 65 V).

The narrow grooves generated by the third body ploughing action [44] can be clearly observed for all the coatings. The removal of loosely bound defects from all the coatings as well as removal of coating material from the coating deposited at U_b = - 40 V produced wear debris which subsequently damaged the surface of the coatings.

Fig. 11a represents the SEM image of the wear track showing voids, generated due to the removal of coating defects during the test. High magnification SEM image of such void can be seen in Fig. 11b.

Although the μ values were not directly influenced by the surface defect density, the study of coating surfaces at higher magnification indicated that it influenced the K_C values of the coatings.

In addition, the bilayer thickness (Δ) of the coatings can also influence the wear resistance [45–53]. The earlier study indicated that the tribological properties, specifically coefficient of wear values depend on crystallographic orientation of the coatings [16]. However, deeper understanding recommends that the layer structure of multilayer coatings influences the wear properties more and crystallographic orientation does influence the tribological properties by influencing the oxidation behaviour during sliding.

The bilayer thickness is a function of the deposition rate [41]. As discussed earlier (sec 3.1), the bias voltage applied to the substrate influenced the deposition rate. Subsequently, it caused similar variation in the bilayer thickness of the coatings. As seen from the Fig. 12, the bilayer thickness of the coating deposited at - 65 V substrate bias was higher (Δ = 27.3 Å) than the other coatings. Interestingly, this coating (U_b = - 65 V) provided the best resistance against wear. While for the coatings deposited with U_b = - 40 V, -100 V, -150 V, the bilayer thicknesses were found to be lower (Δ = 24.9 Å, 25.4 Å and 21.9 Å respectively). Although, the coatings produced at U_b = - 40 V and - 100 V had similar coating thickness (2.02 μm and 2.05 μm) as well as similar bilayer thickness (24.9 Å and 25.4 Å), a significant difference in

their wear values was noticed (4.19×10^{-15} $m^3N^{-1}m^{-1}$ and 3.63×10^{-15} $m^3N^{-1}m^{-1}$ respectively). It could be due to the difference in hardness of the coatings. Table 3 presents the results from the nanoindentation tests of the coatings deposited by varying bias voltage.

As seen from the table, the coating produced with the lowest bias voltage of - 40 V had the lowest hardness value (19.74 GPa). Further increase of bias voltage raised the bombarding energy which led to a higher adhesion between the sputtered atoms and substrate as well as within the columns. As a result, the hardness of the coatings was increased and reached the maximum value (27.39 GPa for U_b = - 100 V). The higher hardness of this coating positively influenced the wear behaviour when compared to the coating deposited at the lowest bias voltage of - 40 V.

Conclusion

CrN/NbN multilayer coatings were deposited by varying the bias voltage to study the effect of bias voltage on defect generation as well as to understand the influence of these defects on corrosion and tribological properties of HIPIMS/UBM coatings. Increase in the bias voltage from - 40 V to - 150 V resulted in an increase in surface defect density from 3.13 % to 4.30 %. Nevertheless, as estimated the microstructure, coating thickness, roughness, bilayer thickness and hardness of the coatings were also influenced by the bias voltage applied to the substrates. The corrosion study confirmed the positive influence of dense microstructure on the barrier properties of the coatings. In the anodic potential range, the corrosion current density was significantly lower for the coatings produced at higher negative bias voltages ($U_b \geq$ - 65 V). However, the effect of coating defects was also apparent. Corrosion curves of the coatings with higher defects exhibited sharp increase in current densities due to the removal of loosely bound defects. The wear mechanism of the coatings was dominated by the removal of coating defects during the tests as well as by the bilayer thickness and coating hardness.

The coating with the maximum bilayer thickness had the lowest wear rate. Raman study on wear tracks suggested that the tribological friction values of the coatings were dependant on the nature of oxides produced during the tests. In this study, - 65 V was found to be the optimum bias voltage to produce coatings with low friction, low wear rates and higher corrosion resistance.

Acknowledgement

This study was carried out within a PhD research programme. The financial support by Zimmer-Biomet (E12093B/JS/BB) is gratefully acknowledged.

Reference:

[1] D.B. Lewis, S.J. Creasey, C. Wustefeld, A.P. Ehiasarian, P.E. Hovsepian, The role of the growth defects on the corrosion resistance of CrN/NbN superlattice coatings deposited at low temperatures, Thin Solid Films. 503 (2006) 143–148. doi:10.1016/j.tsf.2005.08.375.

[2] J.A. Araujo, G.M. Araujo, R.M. Souza, A.P. Tschiptschin, Effect of periodicity on hardness and scratch resistance of CrN/NbN nanoscale multilayer coating deposited by cathodic arc technique, Wear. 330–331 (2015) 469–477. doi:10.1016/j.wear.2015.01.051.

[3] A. Illana, S. Mato, A. Ehiasarian, Y. Purandare, M.I. Lasanta, M.T. de Miguel, P. Hovsepian, F.J. Pérez-Trujillo, Substrate Finishing and Niobium Content Effects on the High-Temperature Corrosion Resistance in Steam Atmosphere of CrN/NbN Superlattice Coatings Deposited by PVD-HIPIMS, Oxid. Met. 87 (2017) 455–467. doi:10.1007/s11085-016-9701-5.

[4] R. Ramadoss, N. Kumar, S. Dash, D. Arivuoli, A.K. Tyagi, Wear mechanism of CrN/NbN superlattice coating sliding against various counterbodies, Int. J. Refract.

Met. Hard Mater. 41 (2013) 547–552. doi:10.1016/j.ijrmhm.2013.07.005.

[5] J.H. Hsieh, C. Li, A.L.K. Tan, C.K. Poh, N.J. Tan, Study of oxidation and wear behaviors of (Nb,Cr)N thin films using Raman spectroscopy, Surf. Coatings Technol. 177–178 (2004) 299–305. doi:10.1016/j.surfcoat.2003.09.008.

[6] H.W. Wang, M.M. Stack, S.B. Lyon, P. Hovsepian, W.D. Münz, The corrosion behaviour of macroparticle defects in arc bond-sputtered CrN/NbN superlattice coatings, Surf. Coatings Technol. 126 (2000) 279–287. doi:10.1016/S0257-8972(00)00554-5.

[7] Y.P. Purandare, A.P. Ehiasarian, M.M. Stack, P.E. Hovsepian, CrN/NbN coatings deposited by HIPIMS: A preliminary study of erosion-corrosion performance, Surf. Coatings Technol. 204 (2010) 1158–1162. doi:10.1016/j.surfcoat.2009.11.006.

[8] Y.P. Purandare, A.P. Ehiasarian, P.E. Hovsepian, Deposition of nanoscale multilayer CrN/NbN physical vapor deposition coatings by high power impulse magnetron sputtering, J. Vac. Sci. Technol. A Vacuum, Surfaces, Film. 26 (2008) 288–296. doi:10.1116/1.2839855.

[9] B. Biswas, Y. Purandare, A.A. Sugumaran, D.A.L. Loch, S. Creasey, A.P. Ehiasarian, P.E. Hovsepian, I. Khan, Defect growth in multilayer chromium nitride/niobium nitride coatings produced by combined high power impulse magnetron sputtering and unbalance magnetron sputtering technique, Thin Solid Films. 636 (2017) 558–566. doi:10.1016/j.tsf.2017.06.027.

[10] M. Lattemann, A.P. Ehiasarian, J. Bohlmark, P.Å.O. Persson, U. Helmersson, Investigation of high power impulse magnetron sputtering pretreated interfaces for adhesion enhancement of hard coatings on steel, Surf. Coatings Technol. 200 (2006) 6495–6499. doi:10.1016/j.surfcoat.2005.11.082.

[11] J. Lin, J.J. Moore, W.D. Sproul, B. Mishra, J.A. Rees, Z. Wu, R. Chistyakov, B.

Abraham, Ion energy and mass distributions of the plasma during modulated pulse power magnetron sputtering, Surf. Coatings Technol. 203 (2009) 3676–3685. doi:10.1016/j.surfcoat.2009.05.048.

[12] A.P. Ehiasarian, Fundamentals and applications of HIPIMS, in: R. Wei (Ed.), Plasma Surf. Eng. Res. Its. Pract. Appl. Res. Signpost, Trivandrum, India, 2008: pp. 35–86.

[13] J. Alami, P.O.Å. Persson, D. Music, J.T. Gudmundsson, J. Bohlmark, U. Helmersson, Ion-assisted physical vapor deposition for enhanced film properties on nonflat surfaces, J. Vac. Sci. Technol. A Vacuum, Surfaces, Film. 23 (2005) 278–280. doi:10.1116/1.1861049.

[14] T. Shimizu, H. Komiya, Y. Teranishi, K. Morikawa, H. Nagasaka, M. Yang, Pressure dependence of (Ti, Al)N film growth on inner walls of small holes in high-power impulse magnetron sputtering, Thin Solid Films. 624 (2017) 189–196. doi:10.1016/j.tsf.2016.09.041.

[15] P.E. Hovsepian, A.A. Sugumaran, Y. Purandare, D.A.L. Loch, A.P. Ehiasarian, Effect of the degree of high power impulse magnetron sputtering utilisation on the structure and properties of TiN films, Thin Solid Films. 562 (2014) 132–139. doi:10.1016/j.tsf.2014.04.002.

[16] B. Biswas, Y. Purandare, A. Sugumaran, I. Khan, P.E. Hovsepian, Effect of chamber pressure on defect generation and their influence on corrosion and tribological properties of HIPIMS deposited CrN/NbN coatings, Surf. Coatings Technol. (2017). doi:10.1016/j.surfcoat.2017.08.021.

[17] V. Vasanthipillay, K. Vijayalakshmi, Influence of Sputter Deposition Time on the Growth of c-Axis Oriented AlN / Si Thin Films for Microelectronic Application, 2012 (2012) 724–729.

[18] E. Penilla, J. Wang, Pressure and Temperature Effects on Stoichiometry and

Microstructure of Nitrogen-Rich TiN Thin Films Synthesized via Reactive Magnetron DC-Sputtering, J. Nanomater. 2008 (2008) 1–9. doi:10.1155/2008/267161.

[19] L. Shan, Y. Wang, J. Li, J. Chen, Effect of N2 flow rate on microstructure and mechanical properties of PVD CrNx coatings for tribological application in seawater, Surf. Coatings Technol. 242 (2014) 74–82. doi:10.1016/j.surfcoat.2014.01.021.

[20] I. Petrov, P.B. Barna, L. Hultman, J.E. Greene, Microstructural evolution during film growth, J. Vac. Sci. Technol. A Vacuum, Surfaces, Film. 21 (2003) S117. doi:10.1116/1.1601610.

[21] D. Bhaduri, A. Ghosh, S. Gangopadhyay, S. Paul, Effect of target frequency, bias voltage and bias frequency on microstructure and mechanical properties of pulsed DC CFUBM sputtered TiN coating, Surf. Coatings Technol. 204 (2010) 3684–3697. doi:10.1016/j.surfcoat.2010.04.047.

[22] S. Gangopadhyay, R. Acharya, A.K. Chattopadhyay, S. Paul, Effect of substrate bias voltage on structural and mechanical properties of pulsed DC magnetron sputtered TiN-MoSx composite coatings, Vacuum. 84 (2010) 843–850. doi:10.1016/j.vacuum.2009.11.010.

[23] J.-W. Lee, S.-K. Tien, Y.-C. Kuo, C.-M. Chen, The mechanical properties evaluation of the CrN coatings deposited by the pulsed DC reactive magnetron sputtering, Surf. Coatings Technol. 200 (2006) 3330–3335. doi:10.1016/j.surfcoat.2005.07.047.

[24] H. Du, J. Xiong, H. Zhao, Y. Wu, W. Wan, L. Wang, Structure and properties of TiAlLaN films deposited at various bias voltages, Appl. Surf. Sci. 292 (2014) 688–694. doi:10.1016/j.apsusc.2013.12.035.

[25] V.D. Ovcharenko, A.S. Kuprin, G.N. Tolmachova, I.V. Kolodiy, A. Gilewicz, O. Lupicka, J. Rochowicz, B. Warcholinski, Deposition of chromium nitride coatings using vacuum arc plasma in increased negative substrate bias voltage, Vacuum. 117

(2015) 27–34. doi:10.1016/j.vacuum.2015.04.008.

[26] X.S. Wan, S.S. Zhao, Y. Yang, J. Gong, C. Sun, Effects of nitrogen pressure and pulse bias voltage on the properties of Cr-N coatings deposited by arc ion plating, Surf. Coatings Technol. 204 (2010) 1800–1810. doi:10.1016/j.surfcoat.2009.11.021.

[27] P. Panjan, M. Čekada, M. Panjan, D. Kek-Merl, Growth defects in PVD hard coatings, Vacuum. 84 (2009) 209–214. doi:10.1016/j.vacuum.2009.05.018.

[28] A. Drnovšek, P. Panjan, M. Panjan, M. Čekada, The influence of growth defects in sputter-deposited TiAlN hard coatings on their tribological behavior, Surf. Coatings Technol. 288 (2016) 171–178. doi:10.1016/j.surfcoat.2016.01.021.

[29] M. Tkadletz, C. Mitterer, B. Sartory, I. Letofsky-Papst, C. Czettl, C. Michotte, The effect of droplets in arc evaporated TiAlTaN hard coatings on the wear behavior, Surf. Coatings Technol. 257 (2014) 95–101. doi:10.1016/j.surfcoat.2014.01.010.

[30] S. Creasey, D.B. Lewis, I.J. Smith, W.-D. Münz, SEM image analysis of droplet formation during metal ion etching by a steered arc discharge, Surf. Coatings Technol. 97 (1997) 163–175. doi:10.1016/S0257-8972(97)00137-0.

[31] D.D. La Grange, N. Goebbels, A. Santana, R. Heuberger, T. Imwinkelried, L. Eschbach, A. Karimi, Effect of niobium onto the tribological behavior of cathodic arc deposited Nb–Ti–N coatings, Wear. 368–369 (2016) 60–69. doi:10.1016/j.wear.2016.09.003.

[32] P. Souček, J. Daniel, J. Hnilica, K. Bernátová, L. Zábranský, V. Buršíková, M. Stupavská, P. Vašina, Superhard nanocomposite nc-TiC/a-C:H coatings: The effect of HiPIMS on coating microstructure and mechanical properties, Surf. Coatings Technol. 311 (2017) 257–267. doi:10.1016/j.surfcoat.2017.01.021.

[33] Q. Ma, L. Li, Y. Xu, J. Gu, L. Wang, Y. Xu, Effect of bias voltage on TiAlSiN nanocomposite coatings deposited by HiPIMS, Appl. Surf. Sci. 392 (2017) 826–833.

doi:10.1016/j.apsusc.2016.09.028.

[34] A.P. Ehiasarian, P.E. Hovsepian, W.-D. Münz, Combined coating process comprising magnetic field-assisted, high-power, pulsed cathode sputtering and an unbalanced magnetron, Patent US7081186 B2 (25 Jul 2006), EP1260603 A2 (27 Nov 2002), DE10124749 A1 (28 Nov 2002), n.d.

[35] P.E. Hovsepian, D.B. Lewis, W.D. Münz, S.B. Lyon, M. Tomlinson, Combined cathodic arc/unbalanced magnetron grown CrN/NbN superlattice coatings for corrosion resistant applications, Surf. Coatings Technol. 120–121 (1999) 535–541. doi:10.1016/S0257-8972(99)00439-9.

[36] C.P. Constable, J. Yarwood, P. Hovsepian, L.A. Donohue, D.B. Lewis, W.-D. Münz, Structural determination of wear debris generated from sliding wear tests on ceramic coatings using Raman microscopy, J. Vac. Sci. Technol. A Vacuum, Surfaces, Film. 18 (2000) 1681–1689. doi:10.1116/1.582407.

[37] S. Akkaya, B. Yıldız, M. Ürgen, Orientation dependent tribological behavior of TiN coatings., J. Phys. Condens. Matter. 28 (2016) 134009. doi:10.1088/0953-8984/28/13/134009.

[38] T. Wang, G. Zhang, B. Jiang, Comparison in mechanical and tribological properties of CrTiAlMoN and CrTiAlN nano-multilayer coatings deposited by magnetron sputtering, Appl. Surf. Sci. 363 (2016) 217–224. doi:10.1016/j.apsusc.2015.12.005.

[39] C. Tritremmel, R. Daniel, H. Rudigier, P. Polcik, C. Mitterer, Mechanical and tribological properties of Al-Ti-N/Al-Cr-B-N multilayer films synthesized by cathodic arc evaporation, Surf. Coatings Technol. 246 (2014) 57–63. doi:10.1016/j.surfcoat.2014.03.005.

[40] J. Lin, X. Zhang, Y. Ou, R. Wei, The structure, oxidation resistance, mechanical and tribological properties of CrTiAlN coatings, Surf. Coatings Technol. 277 (2015) 58–

66. doi:10.1016/j.surfcoat.2015.07.013.

[41] D.C. Cameron, R. Aimo, Z.H. Wang, K.A. Pischow, Structural variations in CrN/NbN superlattices, Surf. Coatings Technol. 142 (2001) 567–572. doi:10.1016/S0257-8972(01)01057-X.

[42] R. Bes, S. Gavarini, N. Millard-Pinard, S. Cardinal, A. Perrat-Mabilon, C. Peaucelle, T. Douillard, Influence of crystallographic orientation on the early stages of oxidation of polycrystalline titanium nitride, J. Nucl. Mater. 427 (2012) 415–417. doi:10.1016/j.jnucmat.2012.03.031.

[43] M.N. Gardos, Magn´ eli phases of anion-deficient rutile as lubricious oxides. Part I. Tribological behavior of single-crystal and polycrystalline rutile (TinO2n−1), Tribol. Lett. 8 (2000) 65–78. doi:10.1002/andp.200410099.

[44] A.P. Ehiasarian, P.E. Hovsepian, L. Hultman, U. Helmersson, Comparison of microstructure and mechanical properties of chromium nitride-based coatings deposited by high power impulse magnetron sputtering and by the combined steered cathodic arc/unbalanced magnetron technique, Thin Solid Films. 457 (2004) 270–277. doi:10.1016/j.tsf.2003.11.113.

[45] Y.J. Kim, T.J. Byun, H.Y. Lee, J.G. Han, Effect of bilayer period on CrN/Cu nanoscale multilayer thin films, Surf. Coatings Technol. 202 (2008) 5508–5511. doi:10.1016/j.surfcoat.2008.06.028.

[46] M.I. Yousaf, V.O. Pelenovich, B. Yang, C.S. Liu, D.J. Fu, Effect of bilayer period on structural and mechanical properties of nanocomposite TiAlN/MoN multilayer films synthesized by cathodic arc ion-plating, Surf. Coatings Technol. 282 (2015) 94–102. doi:10.1016/j.surfcoat.2015.10.018.

[47] H. Holleck, V. Schier, Multilayer PVD coatings for wear protection, Surf. Coatings Technol. 76–77 (1995) 328–336. doi:10.1016/0257-8972(95)02555-3.

[48] L. Chen, Y.X. Xu, Y. Du, Y. Liu, Effect of bilayer period on structure, mechanical and thermal properties of TiAlN/AlTiN multilayer coatings, Thin Solid Films. 592 (2015) 207–214. doi:10.1016/j.tsf.2015.09.029.

[49] M. Kot, W.A. Rakowski, Major, R. Major, J. Morgiel, Effect of bilayer period on properties of Cr/CrN multilayer coatings produced by laser ablation, Surf. Coatings Technol. 202 (2008) 3501–3506. doi:10.1016/j.surfcoat.2007.12.036.

[50] F. Ge, X. Zhou, F. Meng, Q. Xue, F. Huang, Tribological behavior of VC/Ni multilayer coatings prepared by non-reactive magnetron sputtering, Tribol. Int. 99 (2016) 140–150. doi:10.1016/j.triboint.2015.10.019.

[51] S. Kim, E. Kim, D. Kim, J. La, S. Lee, Effects of Bilayer Period on the Microhardness and Its Strengthening Mechanism of CrN / AlN Superlattice Coatings, 45 (2012) 257–263.

[52] Y.J. Kim, T.J. Byun, J.G. Han, Bilayer period dependence of CrN/CrAlN nanoscale multilayer thin films, Superlattices Microstruct. 45 (2009) 73–79. doi:10.1016/j.spmi.2008.12.020.

[53] M.K. Wu, J.W. Lee, Y.C. Chan, H.W. Chen, J.G. Duh, Influence of bilayer period and thickness ratio on the mechanical and tribological properties of CrSiN/TiAlN multilayer coatings, Surf. Coatings Technol. 206 (2011) 1886–1892. doi:10.1016/j.surfcoat.2011.07.045.

Figure Caption

Fig. 1. (a) Planar and (b) cross-sectional SEM image of coating deposited at - 40 V; (c) Planar and (d) cross-sectional SEM image of coating deposited at - 65 V; (e) Planar and (f) cross-sectional SEM image of coating deposited at - 100 V; (g) Planar and (h) cross-sectional SEM image of coating deposited at - 150 V bias voltage.

Fig. 2. (a) Planar view of a nodular shaped defect, (b) Cross-sectional view of a nodular shaped defect, (c) Planar view of an open void defect and (d) Planar view of a pinhole defect.

Fig. 3. (a) Flakes related defect in HIPIMS/UBM coating and (b) EDX spectra of the defect; (c) Droplet in Arc-deposited coating commercially available and (d) EDX spectra of the droplet.

Fig. 4 (a). Optical microscopic image of the coating surface (U_b = - 40 V), (b) Variation of surface area coved by optically visible defects as a function of substrate bias voltage, (c) SEM image of a stainless steel substrate showing substrate pits, and (d) Optical microscopic image of the commercially available arc-PVD CrN/NbN coating.

Fig. 5. Potentiodynamic polarisation curves of the coatings deposited by varying bias voltage.

Fig. 6. Dependence of friction coefficient on the number of revolutions (friction cycles) for the coatings deposited by varying bias voltage.

Fig. 7. Raman spectra obtained from the wear tracks of the coatings deposited at various bias voltages.

Fig. 8. XRD patterns CrN/NbN nanoscale multilayer coatings by varying substrate bias voltage.

Fig. 9. Wear track profiles of the coatings deposited by varying bias voltage.

Fig. 10. Optical image of the wear track of the coating deposited at (a) - 40 V, (b) - 65 V, (c) - 100 V and (d) -150 V.

Fig. 11. (a) SEM image of the wear track and (b) void within the wear track.

Fig. 12. Low angle diffraction peak and corresponding bilayer thickness of the coatings deposited at various substrate bias.

Table caption

Table 1. Coatings thickness as a function of substrate bias voltage.

Table 2. Roughness of the coatings deposited by varying substrate bias voltage.

Table 3. Hardness of the coatings deposited by varying substrate bias voltage.

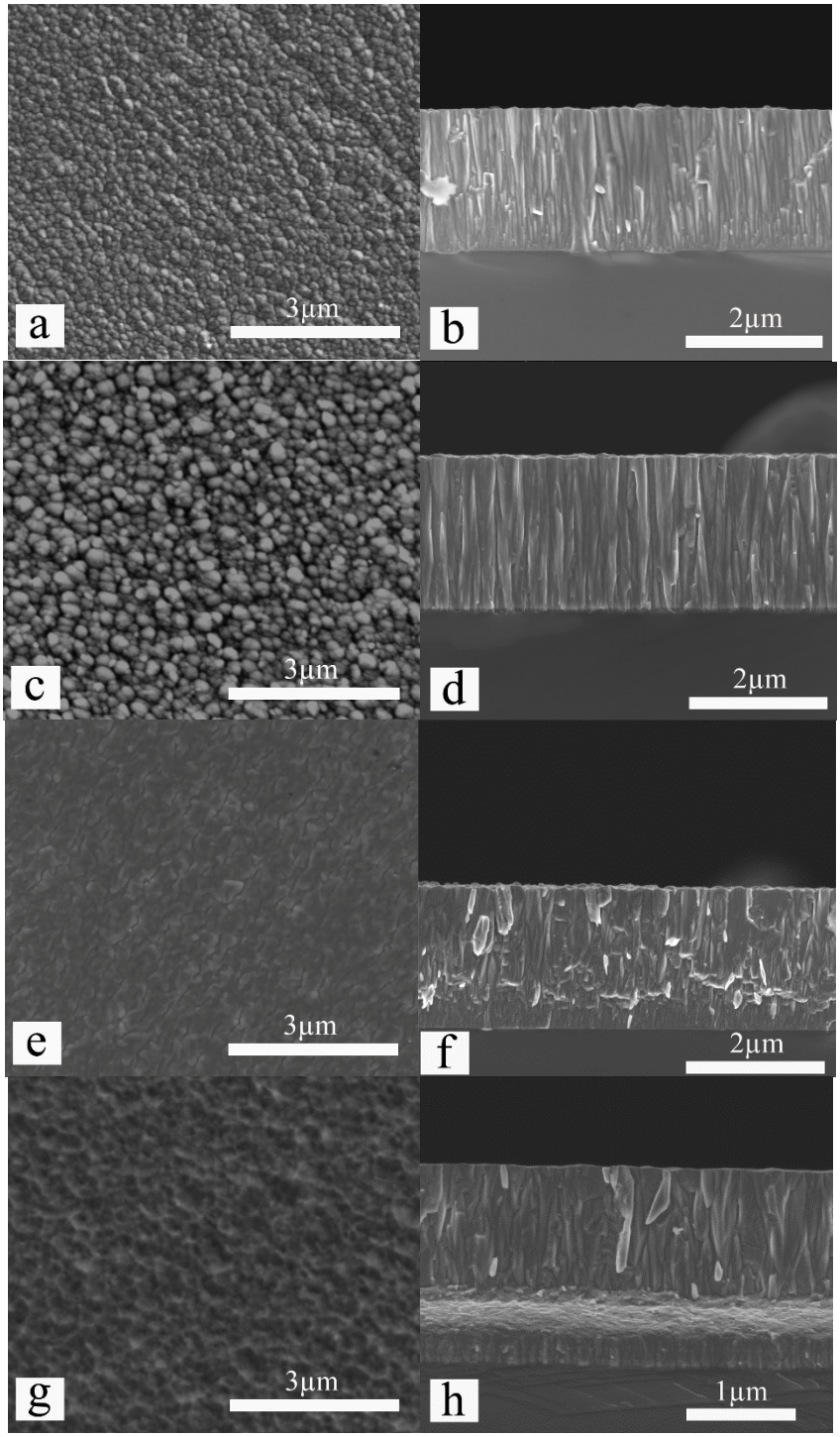

Fig. 1. (a) Planar and (b) cross-sectional SEM image of coating deposited at - 40 V; (c) Planar and (d) cross-sectional SEM image of coating deposited at - 65 V; (e) Planar and (f) cross-sectional SEM image of coating deposited at - 100 V; (g) Planar and (h) cross-sectional SEM image of coating deposited at - 150 V bias voltage.

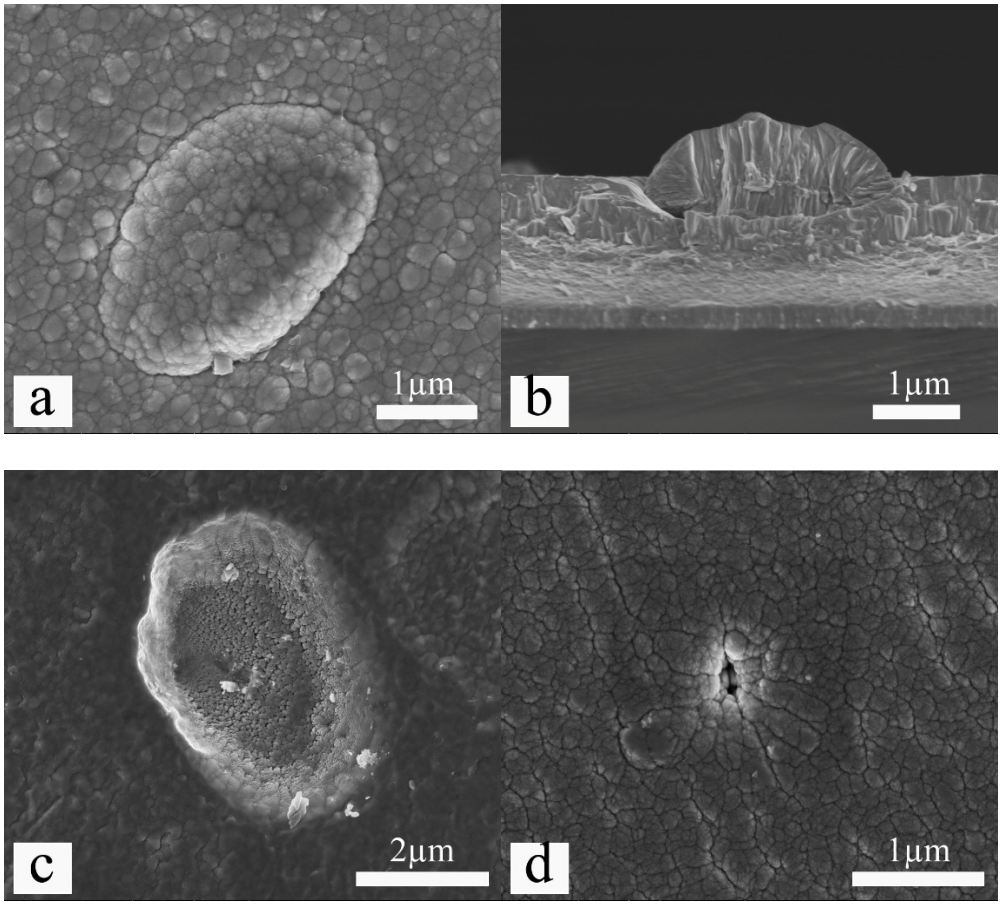

Fig. 2. (a) Planar view of a nodular shaped defect, (b) Cross-sectional view of a nodular shaped defect, (c) Planar view of an open void defect and (d) Planar view of a pinhole defect.

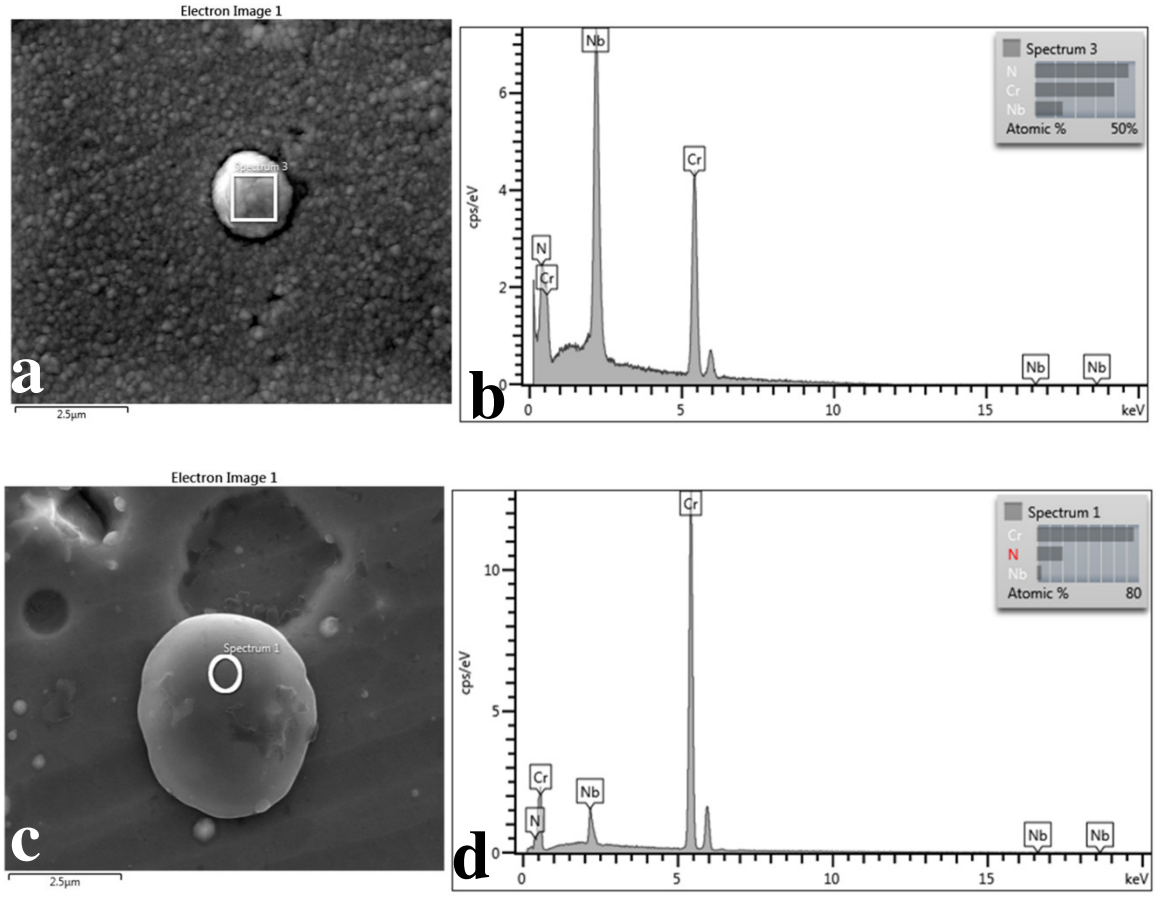

Fig. 3. (a) Flakes related defect in HIPIMS/UBM coating and (b) EDX spectra of the defect; (c) Droplet in Arc-deposited coating commercially available and (d) EDX spectra of the droplet.

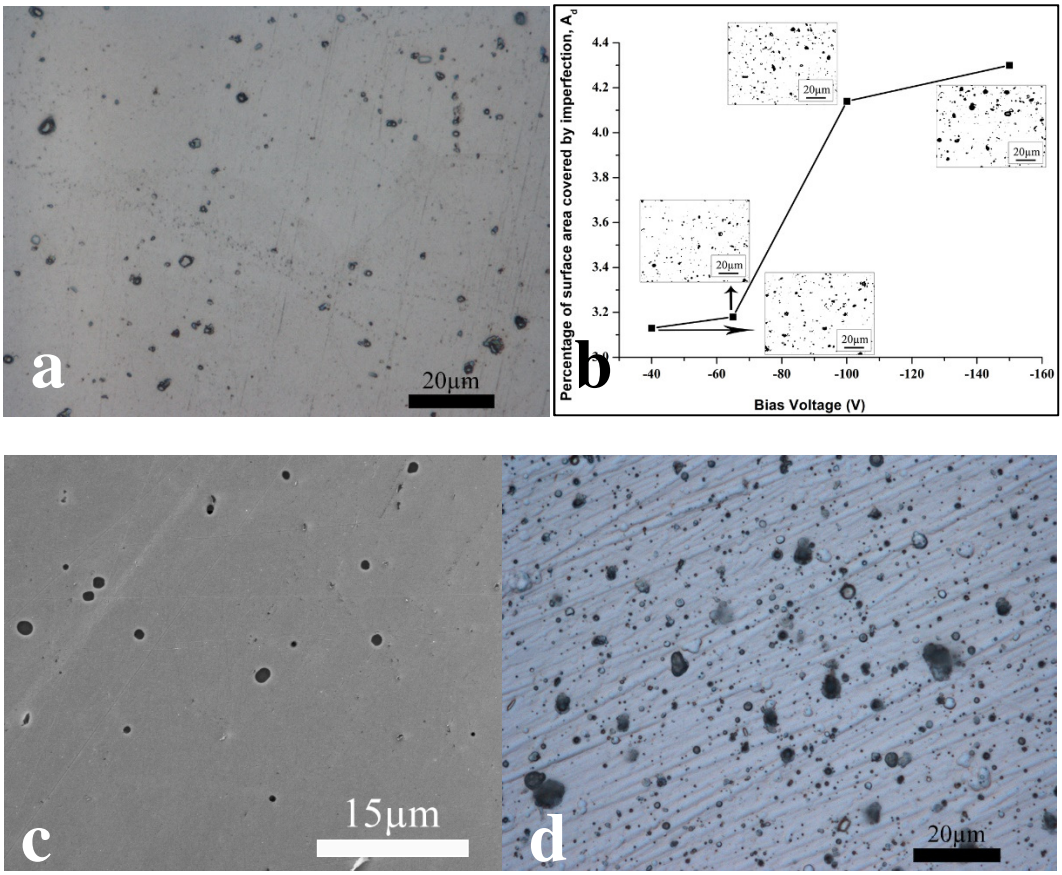

Fig. 4 (a). Optical microscopic image of the coating surface (U_b = - 40 V), (b) Variation of surface area coved by optically visible defects as a function of substrate bias voltage, (c) SEM image of a stainless steel substrate showing substrate pits, and (d) Optical microscopic image of the commercially available arc-PVD CrN/NbN coating.

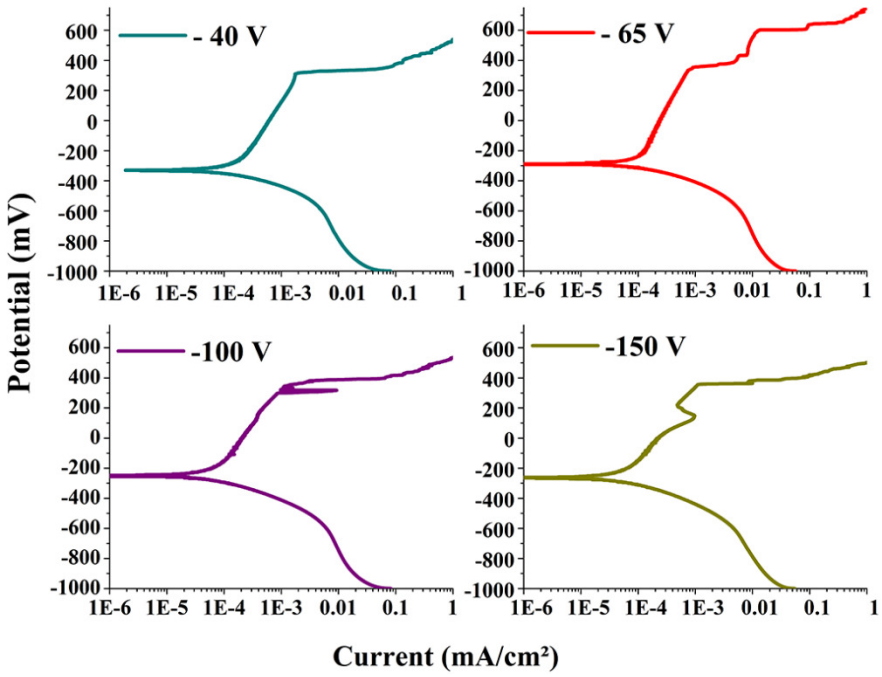

Fig. 5. Potentiodynamic polarisation curves of the coatings deposited by varying bias voltage.

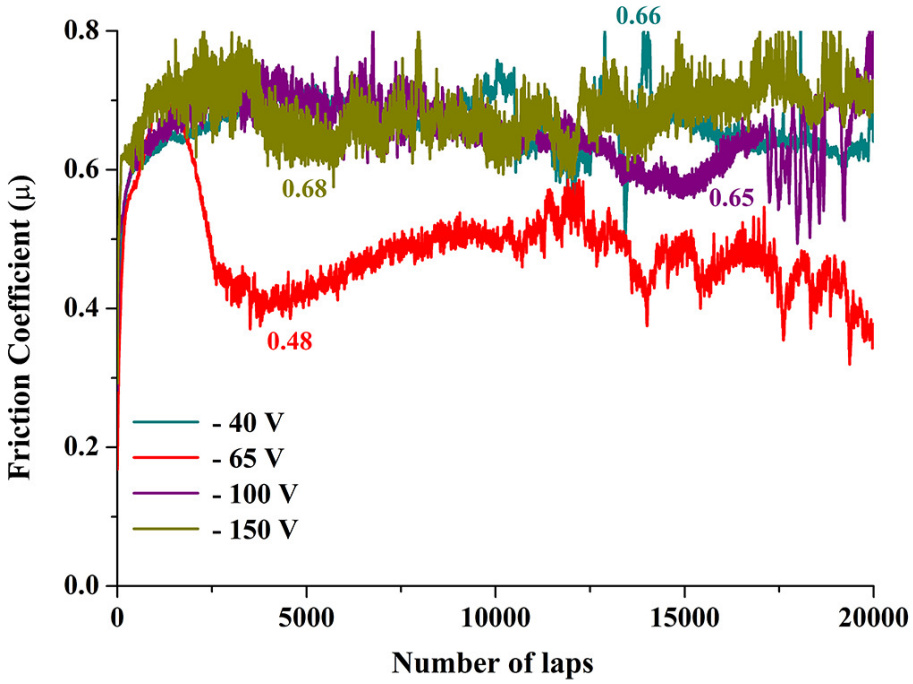

Fig. 6. Dependence of friction coefficient on the number of revolutions (friction cycles) for the coatings deposited by varying bias voltage.

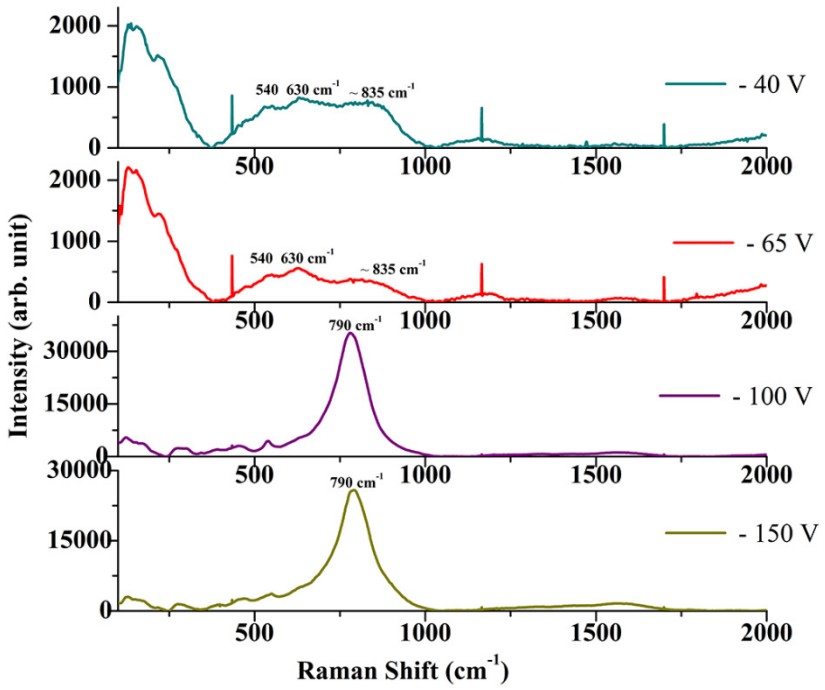

Fig. 7. Raman spectra obtained from the wear tracks of the coatings deposited at various bias voltages.

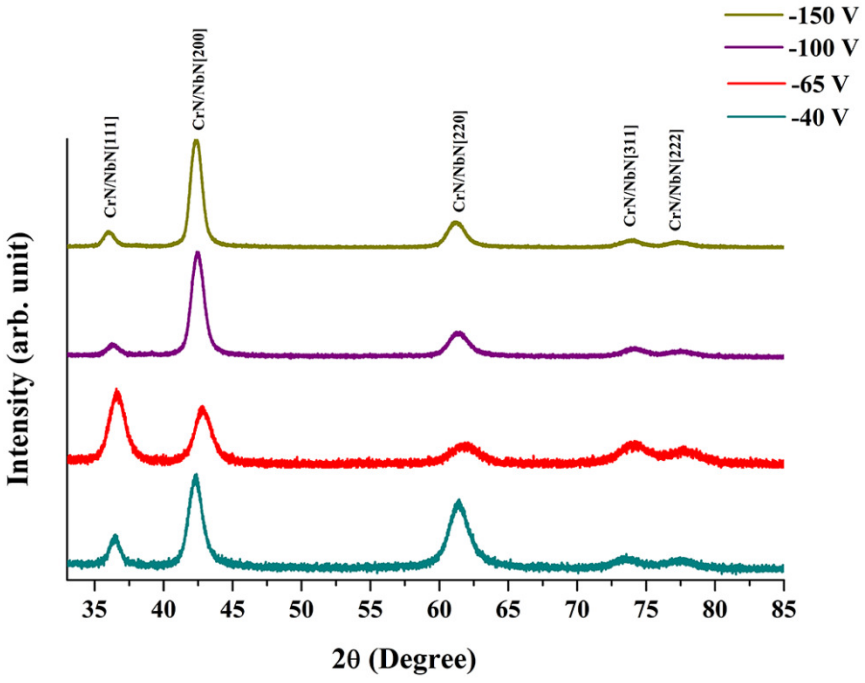

Fig. 8. XRD patterns CrN/NbN nanoscale multilayer coatings by varying substrate bias voltage.

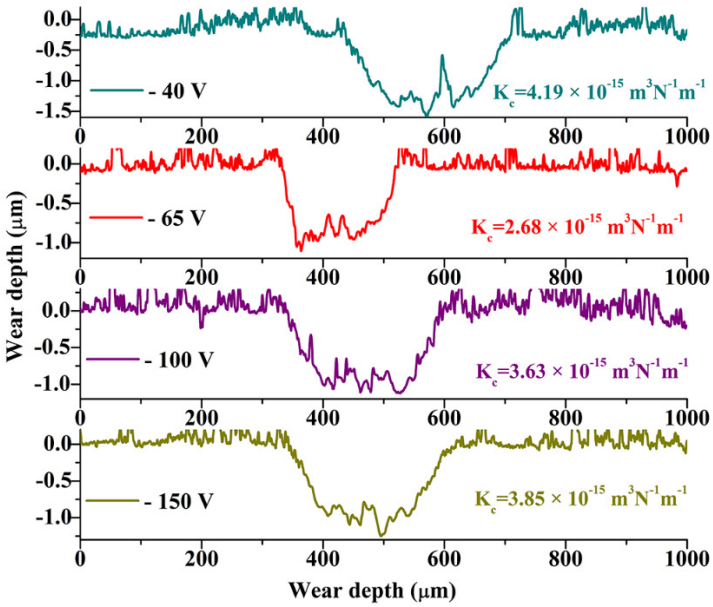

Fig. 9. Wear track profiles of the coatings deposited by varying bias voltage.

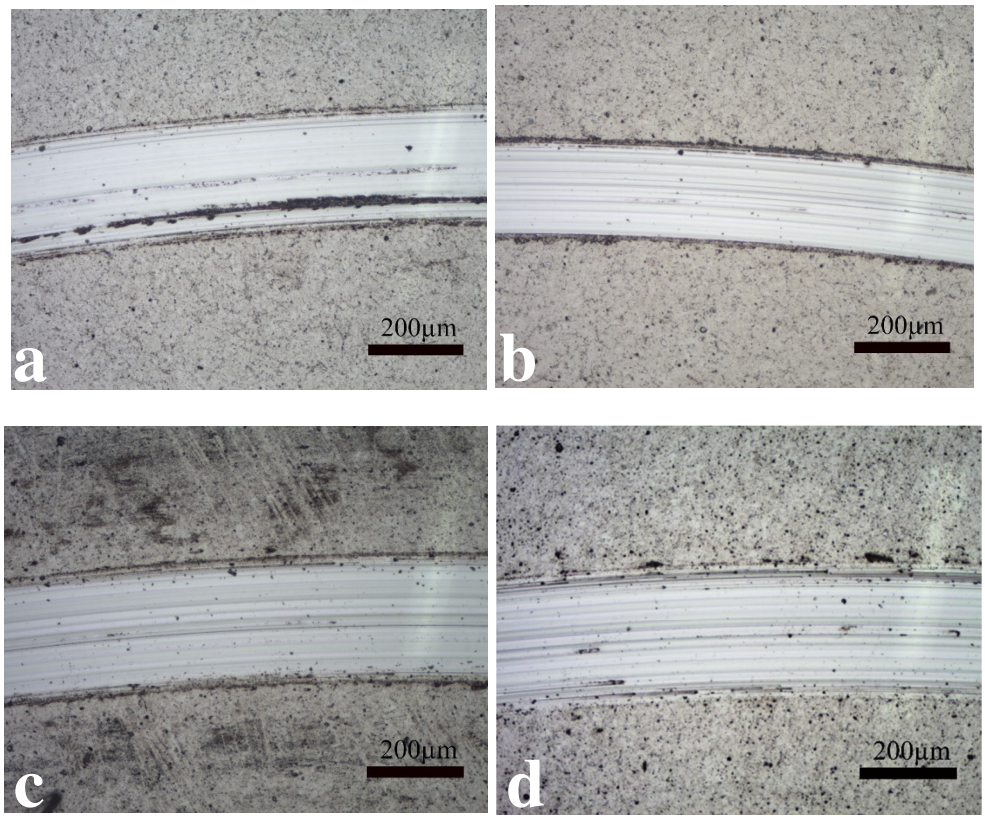

Fig. 10. Optical image of the wear track of the coating deposited at (a) - 40 V, (b) - 65 V, (c) - 100 V and (d) -150 V.

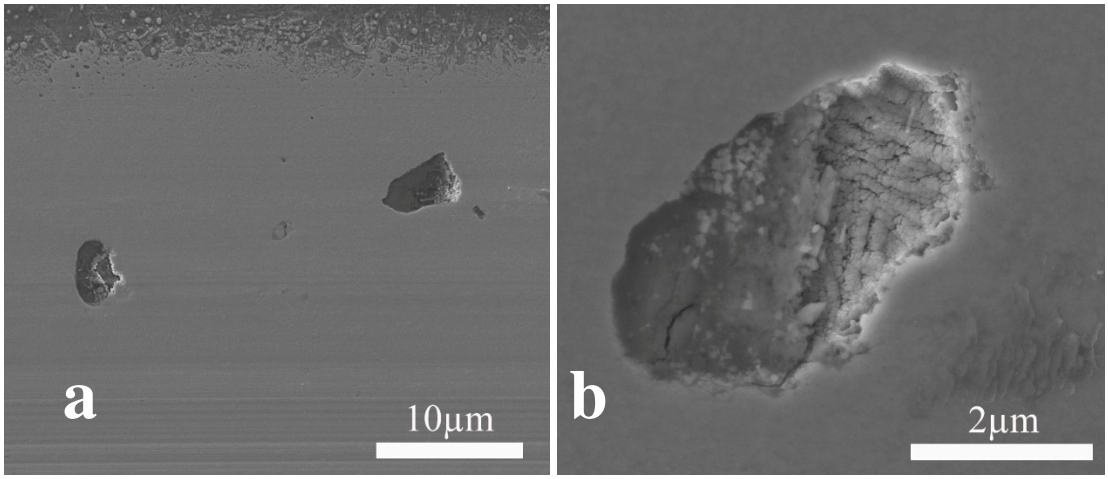

Fig. 11. (a) SEM image of the wear track and (b) void within the wear track.

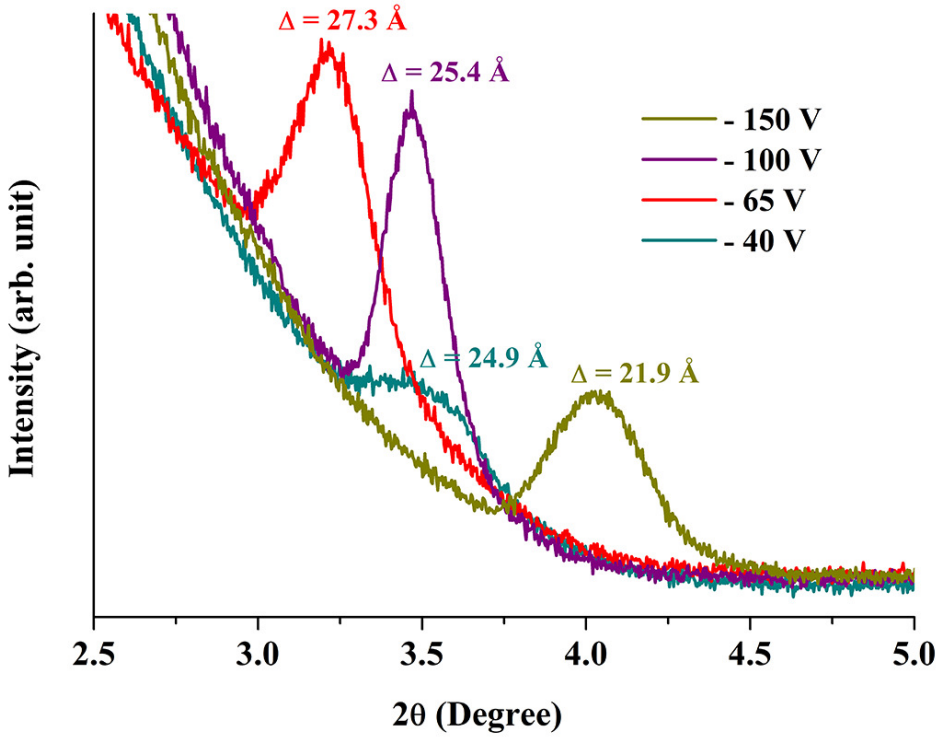

Fig. 12. Low angle diffraction peak and corresponding bilayer thickness of the coatings deposited at various substrate bias.

Bias Voltage (V)	Thickness (µm)
- 40	2.02 ± 0.03
- 65	2.15 ± 0.02
- 100	2.05 ± 0.01
- 150	1.80 ± 0.04

Table 1. Coatings thickness as a function of substrate bias voltage.

Bias Voltage (V)	Roughness (µm)
- 40	0.040
- 65	0.039
- 100	0.083
- 150	0.073

Table 2. Roughness of the coatings deposited by varying substrate bias voltage.

Bias Voltage (V)	Hardness (GPa)
- 40	19.74± 2.4
- 65	25.85± 3.2
- 100	27.39± 3.8
- 150	26.04± 3.9

Table 3. Hardness of the coatings deposited by varying substrate bias voltage.